Available online at www.sciencedirect.com
SCIENCE DIRECT
Trans. Nonferrous Met. Soc. China 18(2008) 890−896
Transactions of Nonferrous Metals Society of China
www.csu.edu.cn/ysxb/

# Effect of second introduced phase on magnetotransport properties of $La_{2/3}Sr_{1/3}MnO_3$/0.33(CuO, ZnO, $Al_2O_3$) composites

ZHOU Zheng-you(周正有)[1], WU Xiao-shan(吴小山)[1, 2], LUO Guang-sheng(罗广圣)[1], JIANG Feng-yi(江风益)[1]

1. School of Materials Science and Engineering, Nanchang University, Nanchang 330031, China;
2. Nanjing National Laboratory of Microstructures, Department of Physics, Nanjing University, Nanjing 210093, China

Received 20 November 2007; accepted 14 March 2008

**Abstract:** The structure, magnetic and magnetotransport properties of $La_{2/3}Sr_{1/3}MnO_3$(LSMO)/0.33(CuO, ZnO, $Al_2O_3$) composites were investigated to explore the role of second introduced phase. The microstructural analysis shows two kinds of grain boundaries: LSMO/LSMO and LSMO/second phase/LSMO. Two maximal resistivities appear in LSMO/0.33CuO and LSMO/0.33ZnO composites while the resistivity of LSMO/0.33$Al_2O_3$ decreases monotonically with increasing the temperature from 200 K to 400 K. Moreover, the temperature dependence of magnetoresistance(MR) of LSMO/0.33$Al_2O_3$ that decreases monotonically with increasing the temperature is different from that of LSMO/0.33CuO and LSMO/0.33ZnO. A developed two-channel model consisting of scattering model and tunneling model was proposed to fit the resistivity—temperature curves of these composites. The role of second introduced phase and the magnetotransport mechanism of these composites were elucidated.

**Key words:** LSMO; magnetoresistance; two-channel model; composites; potential barrier

## 1 Introduction

Manganites exhibit ferromagnetic and metallic properties below Curie transition point because of double exchange(DE) interaction between neighboring $Mn^{3+}$ and $Mn^{4+}$ ions through oxygen sites[1]. The decrease in the resistivity of these compounds at high magnetic fields is attributed to an improvement of spin order and the magnetoresistance(MR) reaches maximal value near the Curie transition($T_c$). The effect of doping ionic radius, doping level and doping sites at either A site or B site in $ABO_3$ perovskite compounds on the magnetotransport properties of the compound has been extensively investigated[2−3]. However, low transition temperature, low room-temperature MR and high magnetic field are enormous challenges for many researchers.

Recently, manganite-based composites have stimulated a surge of researching due to tunneling effect of grain boundaries, which opens a new researching field. In $La_{2/3}Sr_{1/3}MnO_3$ (LSMO) compound, the decrease in resistivity at low magnetic field is attributed to the spin-polarized tunneling across the potential barrier of grain boundaries[4]. Many research groups have prepared manganite-based composites by incorporating some insulating materials, such as $Al_2O_3$[5], $TiO_2$[6], NiO[7], $SiO_2$[8], $CeO_2$[9], $ZrO_2$[10], ZnO [11] and $BaTiO_3$[12−15], into the manganite oxides to explore the effect of second phase on magnetotransport properties of manganites. There are three opinions about the role of second introduced phase in manganite-based composites. ESHRAGHI et al[6−7] attributed the increase in resistivity and the decrease in metal-insulator transition ($T_c$) to the substitution of cations for Mn ions to reduce or dilute the DE interaction. HUESO et al[5] thought that there exists strong electronic scattering created by alumina particles. There are also some reports[16−18] about two-channel model related to intragrain and intergrain conduction. However, the effect of the temperature and potential barrier of grain boundaries on magnetotransport of manganite-based composites has not been considered. If only the spin-dependent scattering and tunneling process dominate the magnetotransport mechanism, the resistivity should increase with the

**Corresponding author:** ZHOU Zheng-you; Tel: +86-791-2941152; +86-13979148440; E-mail: zhouyz@ncu.edu.cn

increase of temperature. However, the resistivity of the composites usually decreases at the temperature above metal-insulator transition temperature($T_p$) up to $T_c$ of pure manganites.

In the present work, the effect of potential barrier between ferromagnetic(FM) and second incorporated phases on magnetotransport properties of manganites-based composites is investigated. Second introduced phases such as CuO, ZnO and $Al_2O_3$ with different bandgap and the same mole ratio are respectively incorporated into LSMO matrix. The effect of temperature on bandgap of second phase and potential barrier of grain boundaries should be neglected compared with large difference in bandgap. A two-channel model composed of parallel scattering model and tunneling model is used to fit the resistivity—temperature curve and the magnetotransport mechanism is elucidated.

## 2 Experimental

The LSMO/0.33(CuO, ZnO, $Al_2O_3$) composites were prepared by three steps. Firstly, LSMO compound was prepared by conventional solid-state reaction method. High-purity powders of $La_2O_3$, $SrCO_3$ and $MnO_2$ were mixed in stoichiometric proportions. The mixture was ball-milled for 4 h, pelletized at a pressure less than 30 MPa and calcinated at 1 100 ℃ for 12 h. The pellet was crushed and ground. The same procedures were repeated twice. X-ray diffraction(XRD) patterns show that the perovskite-like phase was formed. Secondly, the powders of 33%(mole fraction) CuO, ZnO, $Al_2O_3$ were respectively introduced into LSMO matrix and were ground to form a homogeneous powder. Finally, the mixture was pelletized at a pressure of 300 MPa and sintered at 1 250 ℃ for 12 h.

The structures of LSMO/0.33(ZnO, CuO, $Al_2O_3$) samples were characterized by X-ray diffractometer (Cu $K_\alpha$). The microstructures of the samples were taken by HITACHI S−3000N scanning electron microscope (SEM). The magnetotransport properties were measured in a magnetic field range of 0−5 T and a temperature range of 200−400 K using a four-probe method with physical properties measurement system(PPMS).

## 3 Results and discussion

### 3.1 Structures of $La_{2/3}Sr_{1/3}MnO_3$(LSMO)/0.33(CuO, ZnO, $Al_2O_3$) composites

Fig.1 shows the XRD patterns at room temperature for pure LSMO and three doped samples. One can see from Fig.1 that the diffraction peaks related to CuO phase appear. It is hard to see the peaks related to ZnO and $Al_2O_3$ phases. In order to analyze the microstructures of pure and doped samples, the fracture sections of doped samples were examined by SEM, as shown in Fig.2. Compared with pure LSMO compound shown in Fig.2(a), the doped compounds form the second phases such as CuO, ZnO, $Al_2O_3$ on the grain boundaries and grain surfaces of LSMO as shown in Figs.2(b), (c) and (d). ZnO and $Al_2O_3$ doping has no obvious effect on the grain size of LSMO. However, the grain size of LSMO in CuO-doped sample is larger than that of pure and two other doped samples. CuO has a melting point of 1 325 ℃ near the 1 250 ℃ sintering temperature. Liquid sintering promotes the grain growth of LSMO.

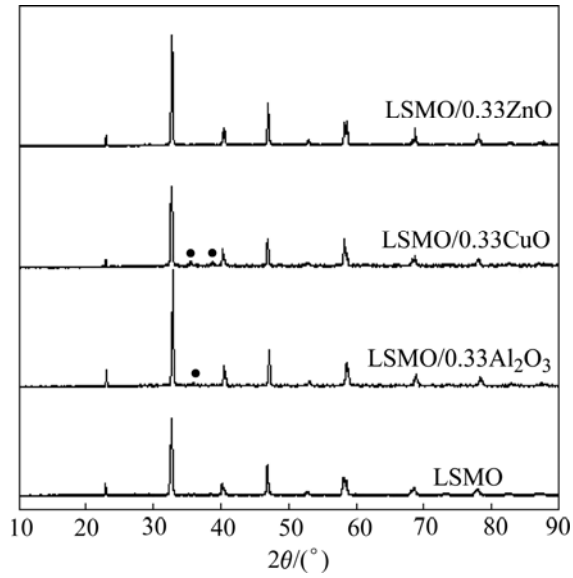


**Fig.1** XRD patterns of pure and CuO, ZnO, $Al_2O_3$ doped LSMO samples

### 3.2 Magnetotransport properties of LSMO/0.33(CuO, ZnO, $Al_2O_3$) composites

The temperature dependence of resistivity of the LSMO/0.33(CuO, ZnO, $Al_2O_3$) is shown in Fig.3. One can see that the resistivity of CuO-doped composite is higher than that of ZnO-doped composites and the resistivity of $Al_2O_3$-doped composite is higher than that of other two systems. There are two peaks in resistivity—temperature curve for CuO-doped and ZnO-doped composites, while the resistivity of $Al_2O_3$-doped composite decreases monotonically with the increase of temperature in the range of 200−400 K. The temperatures of peak resistivity for CuO-doped composites are 360 and 256 K and the temperatures of peak resistivity for ZnO-doped composite are 349 and 259 K. The higher temperature of peak resistivity for CuO-doped and ZnO-doped composites is near the metal-insulator transition point($T_p \approx 369$ K) of LSMO

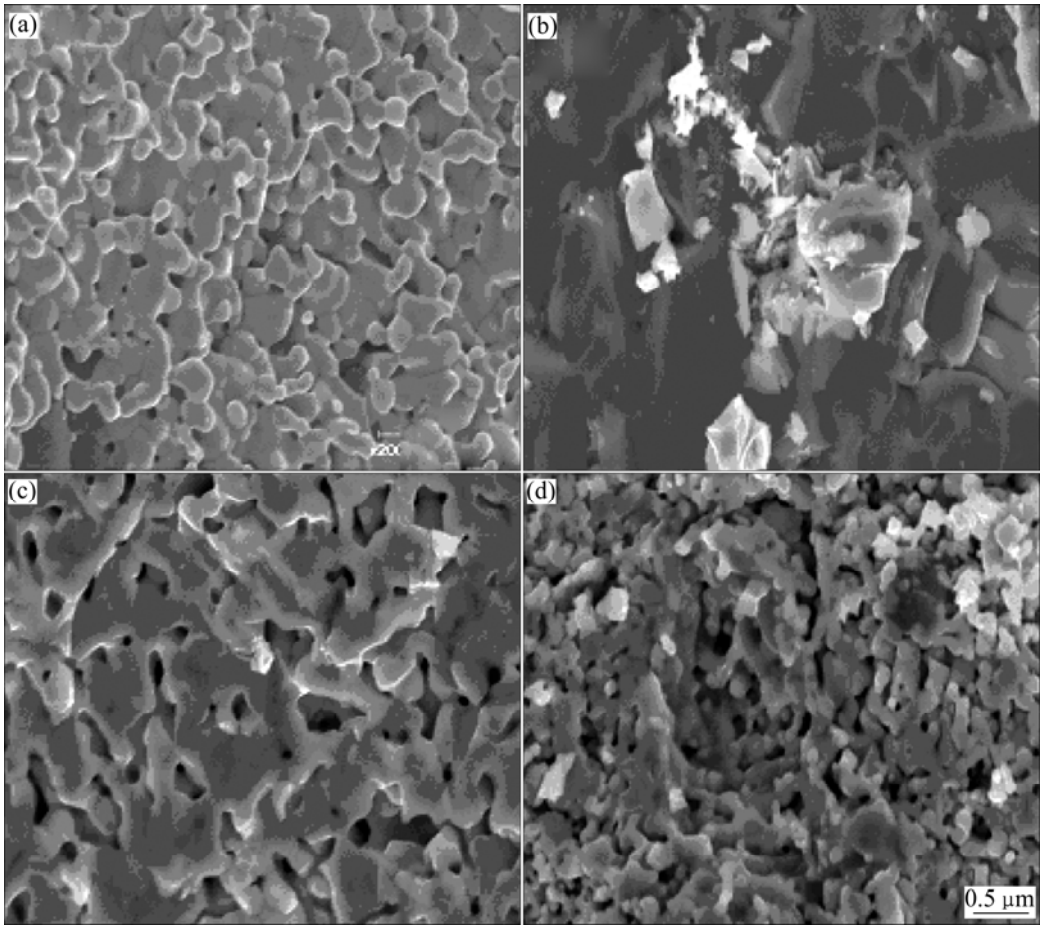


**Fig.2** SEM micrographs of pure and doped LSMO samples: (a) Pure LSMO sample; (b) LSMO/0.33CuO composite; (c) LSMO/0.33ZnO composite; (d) LSMO/0.33$Al_2O_3$ composite

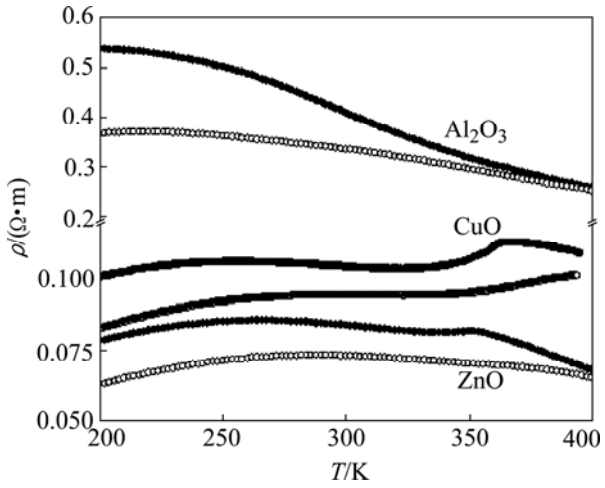


**Fig.3** Temperature dependence of resistivity of LSMO/0.33(CuO, ZnO, $Al_2O_3$) composites

compound and therefore should be the metal-insulator transition temperature($T_p$). Compared with the $T_p$ of LSMO compound, the decrease in $T_p$ of CuO-doped and ZnO-doped composites should be due to the substitution of cations for Mn sites to reduce or dilute the DE interaction between $Mn^{3+}$ and $Mn^{4+}$. How is the low-temperature peak resistivity formed?

### 3.3 Discussion

For manganese oxides, the resistivity($\rho$) increases with the increase of temperature due to temperature-dependent structural disordered scattering and spin-dependent scattering. The variation of $\rho$ with temperature is expressed in the expression $\rho=\rho_0+\rho_1T^2+\rho_3T^{4.5}$, where the temperature independent part $\rho_0$ is the resistivity due to domain, grain boundary and other temperature independent scattering mechanism; $\rho_1T^2$ represents the resistivity due to the electron-electron scattering process. $\rho_3T^{4.5}$ is a combination of electron-electron, electron-magnon and electron-phonon scattering process[19−20]. The equation is used to fit the resistivity—temperature curve in the temperature range of 200−320 K and the fitted curve is almost overlapped with measured curve shown in Fig.4(a). It can not be used to fit the $\rho$—$T$ curve in the range of 200−360 K described in bold line.

There are two kinds of conduction channels

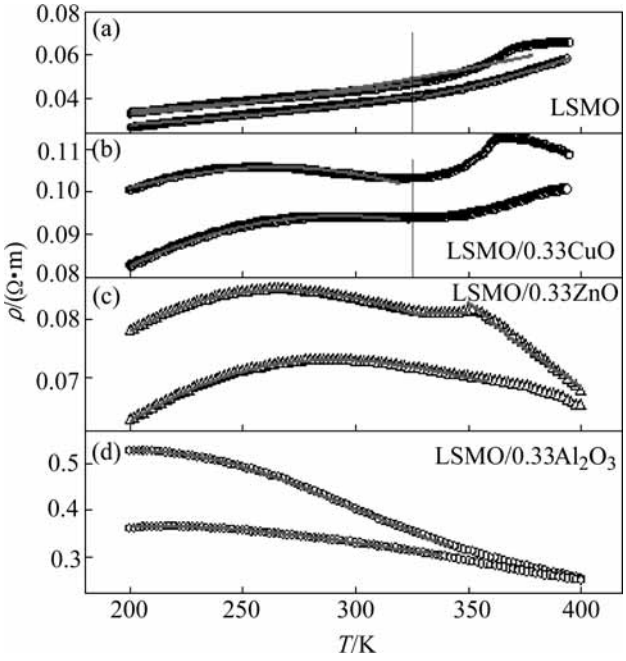


**Fig.4** Fitting curves of polycrystalline LSMO/0.33(CuO, ZnO, $Al_2O_3$) composites with scattering channel and tunneling channel

connected in parallel in polycrystalline manganite-based composites[16−18]. One is related to intragrain and the other is related to intergrain hopping of the conduction electrons between the neighboring sites. There are two kinds of grain boundaries as shown in Fig.5. In channel 1, electrons hop across the boundaries between ferromagnetic(FM) grains. In channel 2, the second phase separates the ferromagnetic grains and forms the sandwich structure of FM/second phase/FM. The total resistivity is expressed as the formation of $1/\rho=1/\rho_{c1}+1/\rho_{c2}$, where $\rho_{c1}$ and $\rho_{c2}$ are the resistivities of channel 1 and channel 2, respectively. For channel 1, electrical behavior is dominated by spin-dependent scattering and grain-boundary scattering. For channel 2, most carriers are scattered by potential barrier of grain boundaries and only few carriers can tunnel through the potential barrier. The scattering channel consists of channel 1 and the scattering part of channel 2. The total resistivity consists of scattering resistivity and tunneling resistivity and is expressed as the formation of $1/\rho=1/\rho_s+1/\rho_t$, where $\rho_s$ and $\rho_t$ are scattering resistivity and tunneling resistivity, respectively. The system of LSMO-based composite is similar to granular system and the variation of tunneling resistivity $\rho_t$ with temperature is expressed in $\rho_t=P_1\times\exp(P_2T^{-1/2})$ equation[21], where $P_1$ and $P_2$ are parameters. The five parameters are obtained by fitting the resistivity—temperature curves of the composite.

The combined transport model is used to fit the $\rho-T$ curves of different composites in the temperature

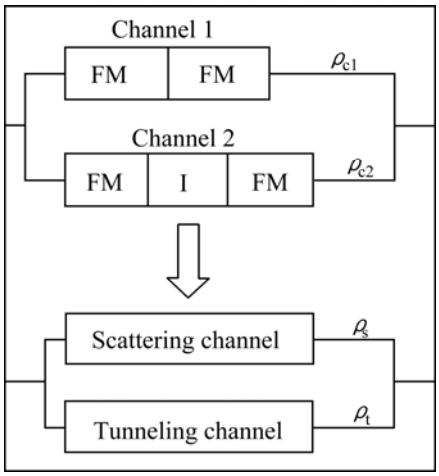


**Fig.5** Two-channel model consisting of scattering channel and tunneling channel for LSMO-based composites

range of 200−320 K shown in Figs.4(b), (c) and (d). To identify the difference between fitted curves and measured curves, bold-solid fitted curves are adopted. One can see that these fitted curves are almost overlapped with experimental data, which indicates that a combined transport model can express the true physical mechanism of these composites in the temperature range of 200−320 K. The electrical behavior of CuO- and ZnO-doped samples in the temperature range of 320−360 K is similar to that of LSMO compound and is not fitted.

The fitted parameters were obtained including parameters of scattering model and tunneling model. These parameters vary with magnetic field and different dopants. The temperature-independent $\rho_0$ increases sharply when the second phase is incorporated. To investigate the effect of the variation of these fitted parameters on resistivity of these compounds, $\rho_1T^2$, $\rho_2T^{4.5}$, $\rho_s$ and $\rho_t$ were calculated respectively according to these fitted parameters in the temperature range of 200−320 K as shown in Fig.6 and Fig.7. One can see from Fig.6 that the value of $\rho_1T^2$ is larger than that of $\rho_2T^{4.5}$ for ZnO doped sample while the value of $\rho_1T^2$ is smaller than that of $\rho_2T^{4.5}$ for CuO and $Al_2O_3$-doped samples. It is well known that $\rho_1T^2$ and $\rho_2T^{4.5}$ represent electron-electron scattering and electron-phonon scattering respectively. Therefore, the bandgap width of second introduced phase affects the potential barrier of grain boundaries and dominates the scattering mechanism.

$\rho_s$ increases and $\rho_t$ decreases with the increase of temperature as shown in Fig.7. For parallel circuit, the total resistivity is dominated by the lower resistivity and smaller than lower resistivity. One can also see that the $\rho_t$ is larger than $\rho_s$ at low temperature and is smaller than $\rho_s$ at high temperatures in these composites. The result indicates that the total resistivity at low temperatures is

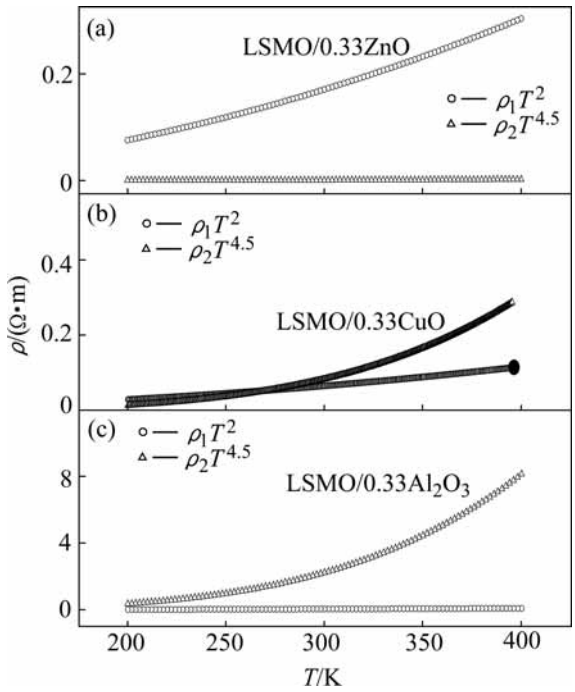


**Fig.6** Calculated $\rho_1T^2$ and $\rho_2T^{4.5}$ for LSMO/0.33(CuO, ZnO, $Al_2O_3$) composites: (a) LSMO/0.33ZnO composite; (b) LSMO/0.33CuO composite; (c) LSMO/0.33$Al_2O_3$ composite

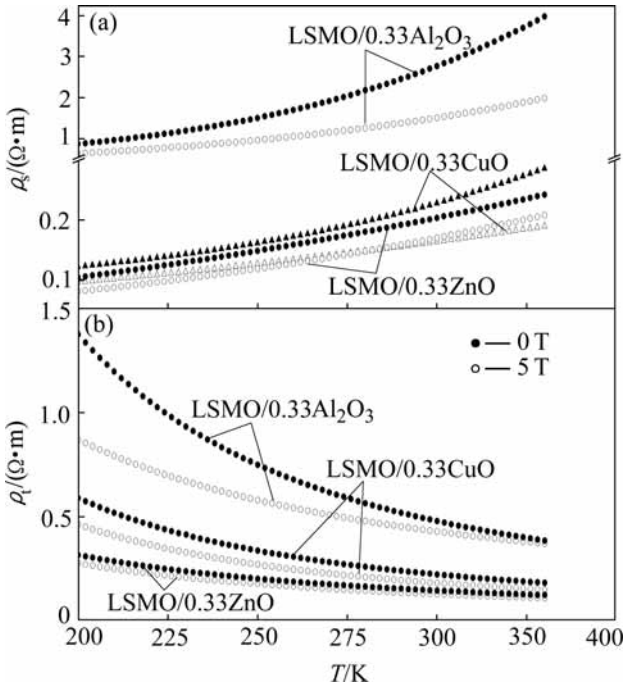


**Fig.7** Calculated scattering resistivity and tunneling resistivity for LSMO/0.33(CuO, ZnO, $Al_2O_3$) composites

controlled by $\rho_s$ and the resistivity is controlled by $\rho_t$ at high temperatures. $\rho$ probably has a peak resistivity at a middle temperature.

For LSMO compound, the scattering mechanism includes structural disordered scattering, grain-boundary scattering and spin-dependent scattering. If second phase is incorporated, electronic grain-boundary scattering and tunneling process occur. Although the room-temperature bandgap of ZnO (3.30 eV) is larger than that of CuO (1.1 eV), ZnO easily collapses to form the Zn interstitionals and O vacancies during sintering process, which is applied in ZnO-based varistor field[22]. Therefore, ZnO ceramic is conductive while CuO ceramic is insulating at room temperature. The potential-barrier scattering between LSMO grains and ZnO grains is very weak and the carriers can tunnel ZnO grains easily, which reduces $\rho_t$. Compared with $\rho_t$ (0.07 Ω·m) of LSMO compounds, the increase in $\rho_s$ (0.1 Ω·m) in ZnO-doped composite should be attributed to grain-boundary scattering between different phases due to structural disorder. $\rho_s$ values at 200 K for CuO-doped and $Al_2O_3$-doped composites are near 0.11 Ω·m and 1.0 Ω·m respectively. These results show that the potential-barrier scattering is enhanced for CuO-doped composite and is dominated for $Al_2O_3$-doped composite. Fig.7(b) shows that the tunneling resistivity for $Al_2O_3$-doped composite decreases sharply with the increase of temperature due to thermal tunneling effect.

At a 5 T high field, the decreasing magnitudes in $\rho_s$ at 200 K for LSMO, ZnO-doped, CuO-doped and $Al_2O_3$-doped composites are about 0.01, 0.02, 0.03 and 0.17 Ω·m, respectively. It is well known that the electrical behavior of channel 1 is similar to that of LSMO compound and the decreasing value in $\rho_s$ due to the improvement of spin order at 200 K is about 0.01 Ω·m. So the decrease in $\rho_s$ of channel 2 makes larger contribution to the decrease in total scattering resistivity and should be attributed to the enhancement of spin-dependent tunneling effect. For $Al_2O_3$-doped composite, the decreasing magnitude in $\rho_s$ is further larger than other two systems, which indicates that spin-dependent tunneling is more obvious for high potential barrier of grain boundaries. The decrease in $\rho_t$ should be the result of improvement of spin order near second phase. At higher temperatures, magnetic field has little effect on $\rho_t$ and $\rho$ due to the spin-disordered alignment.

The temperature-dependent MR for different composites is shown in Fig.8. MR is defined as $100\times(\rho_0-\rho_H)/\rho_0$, where $\rho_H$ and $\rho_0$ represent the resistivity with and without an applied magnetic field respectively. The low-temperature MR increases and high-temperature MR decreases with the increase of potential barrier of grain boundaries. The potential barrier of the grain boundaries between LSMO and ZnO grains is very low because of the conductive property of ZnO. So the MR of ZnO-doped composite is dominated by spin-dependent scattering and tunneling effect. The temperature depen-

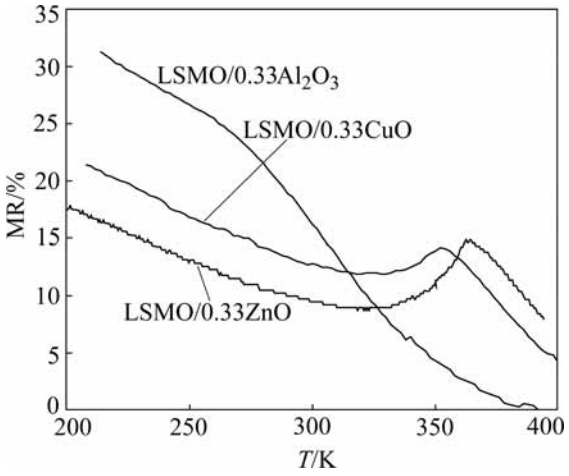


**Fig.8** Temperature dependence of MR for LSMO/0.33(CuO, ZnO, $Al_2O_3$) composites

dence of MR of CuO-doped composites is similar to that of ZnO-doped composite because of low potential barrier of grain boundaries. For $Al_2O_3$-doped composite, the low-temperature MR is dominated only by spin-dependent tunneling and high temperature MR is dominated by thermal tunneling mechanism.

Fig.9 shows the magnetic-field dependence of MR at different temperatures. The low-field MR at 220 K and in a magnetic field of $4\times10^5$A/m shown in Fig.9(a) is almost the same for three composites. For LSMO compound, a sharp decrease in resistivity is attributed to spin- polarized tunneling effect[4]. The low-field MR is enhanced when some second phases are introduced[6−7]. However, the low-field MR disappears in the three composites. It is very difficult for carriers to tunnel across the thick second phase at high doping level and low field, which has been found in other high-level

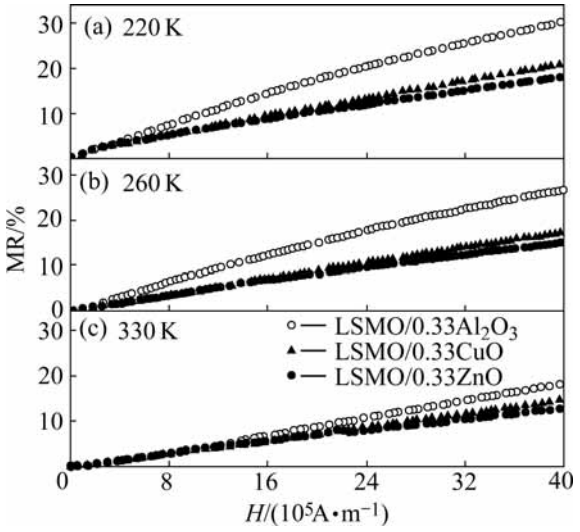


**Fig.9** Magnetic field dependence of MR at different temperatures: (a) 220 K; (b) 260 K; (c) 300 K

doping systems[6−8]. With increasing the magnetic field, the MR of the composites increases. The MR of LSMO/0.33$Al_2O_3$ composite is larger than that of other two composites, which indicates that spin-dependent tunneling through the grain boundaries of different phase is dominated by potential barrier.

## 4 Conclusions

The structure and magnetotransport properties of LSMO/0.33(CuO,ZnO,$Al_2O_3$) composites were investigated. There are two kinds of grain boundaries labeled as LSMO/LSMO and LSMO/second phase/LSMO. The temperature dependence of resistivity and MR of LSMO/0.33$Al_2O_3$ that decreases monotonically is completely different from that of LSMO/0.33CuO and LSMO/0.33ZnO. Two resistivity peaks appear for LSMO/0.33CuO and LSMO/0.33ZnO composites and their value is close to that of LSMO compound. A two-channel model consisting of scattering channel and tunneling channel was developed to fit the measured resistivity—temperature curves. The fitted results show that the total resistivity of LSMO-based composite is dominated by scattering channel at low temperatures and dominated by tunneling channel at high temperatures. The potential barrier of grain boundaries of different phases and bandgap of second phase play an important role in resistivity and MR of the composite. Wide bandgap of second phase increases potential barrier and scattering resistivity, which strengthens spin-dependent tunneling at high magnetic field and low temperature.

## References

[1] ZENER C. Interaction between the *d*-shells in the transition metals (II): Ferromagnetic compounds of manganese with perovskite structure [J]. Phys Rev, 1951, 82: 403−405.

[2] HWANG H Y, CHEONG S W, RADAELL P G, MAREZO M, BATLOGG B. Lattice effects on the magnetoresistance in doped $LaMnO_3$ [J]. Phys Rev Lett, 1995, 75: 914−917.

[3] URASHIBARA A, MORITOMO Y, ARIMA T, ASAMITSU A, KIDO G, TOKURA Y. Insulator-metal transition and giant magnetoresistance in $La_{1-x}Sr_xMnO_3$ [J]. Phys Rev B, 1995, 51: 14103−14109.

[4] FONTCUBERTA J, MARTTLNEZ B, SEFFAR A, GARCIA-MUÑOZ J L, OBRADORS X. Colossal magnetoresistance of ferromagnetic manganites: Structural turning and mechanisms [J]. Phys Rev Lett, 1996, 76: 1122−1125.

[5] HUESO L E, RIVAS J, RIVADULLA F, LOPEZ-QUINTELA M A. Magnetic and intergranular transport properties in manganite/alumina composites [J]. J Non-Crystalline Solids, 2001, 287: 324−328.

[6] KAMELI P, SALAMATI H, ESHRAGHI M, MOHAMMADIZADEH M R. The effect of $TiO_2$ doping on the structure and magnetic and magnetotransport properties of $La_{0.75}Sr_{0.25}MnO_3$ composite [J]. J Appl Phys, 2005, 98: 043908−4.

[7] ESHRAGHI M, SALAMATI H, KAMELI P. The effect of NiO

doping on the structure, magnetic and magnetotransport of $La_{0.8}Sr_{0.2}MnO_3$ composite [J]. J Alloy and Compounds, 2007, 437: 22−26.

[8] DAS D, CHOWDHURY P, DAS R N, SRIVASTAVA C N, NIGAM A K, BAHADUR D. Solution sol-gel processing and investigation of percolation threshold in $La_{2/3}Ca_{1/3}MnO_3$:$x$$SiO_2$ nanocomposite [J]. J Magn Magn Mater, 2006, 238:178−184.

[9] LI B, CARRILLO A E, MARTINEZ B, FONTCUBERTA J. Enhanced field sensitivity close to percolation in magnetoresistive $La_{2/3}Sr_{1/3}MnO_3/CeO_2$ composites [J]. Appl Phys Lett, 1999, 74: 4014−4016.

[10] LU W J, SUN Y P, ZHU X B, SONG W H, DU J J. Low-field magnetoresistance in $La_{0.8}Sr_{0.2}MnO_3/ZrO_2$ composite system [J]. Mater Lett, 2006, 60: 3207−3211.

[11] LEI L W, FU Z Y, ZHANG J Y, WANG H. Synthesis and low field transport properties in a ZnO-doped $La_{0.67}Ca_{0.33}MnO_3$ composites [J]. Mater Sci Eng B, 2006, 128: 70−74.

[12] SHLYAKHTIN O A, OH Y J, TRETYAKOV Y D. Enhanced low field magnetoresistance at room temperature in $La_{0.7}Sr_{0.3}MnO_3$/$SrTiO_3$ composites [J]. Solid State Communications, 2001, 117: 261−266.

[13] WANG C C, LIU W, CUI Y M, ZHANG L W. Effect of sintering temperature on magneto-transport properties of $La_{0.67}Ba_{0.33}MnO_3$/$Ba_{0.7}Sr_{0.3}TiO_3$ composites [J]. Mater Res Bull, 2007, 42: 633−639.

[14] REN G M, YUAN S L, GUAN H G, XIAO X, YU G Q, MIAO J H, WANG Y Q, YIN S Y. Electrical transport and magnetoresistance in $La_{0.67}Ca_{0.33}MnO_3/BaTiO_3$ composites [J]. Mater Lett, 2007, 61: 767−769.

[15] ESA B, TARAN S, KARMAKAR S, CHAUDHURI B K, PAL S, SUN C P, YANG H D. Effect of grain boundary layer strain on the magnetic and transport properties of (100−$x$)$La_{0.7}Ca_{0.3}MnO_3$/($x$)$BaTiO_3$ composites showing enhanced magnetoresistance [J]. J Magn Magn Mater, 2007, 314: 30−36.

[16] HUESO L E, RIVAS J, RIVADULLA F, LOPEZ-QUINTELA M A. Magnetoresistance in manganite/alumina nanocrystalline composites [J]. J Appl Phys, 2001, 89: 1746−1750.

[17] RUBINSTEN J M. Two-component model of polaronic transport [J]. J Appl Phys, 2000, 87: 5019−5021.

[18] DAS D, SRIVASTAVA C M, BAHADUR D, NIGAM A K, MALIK S K. Magnetic and electrical properties of $La_{0.67}Ca_{0.33}MnO_3$(LCMO): $x$ZnO composites [J]. J Phys: Condens Matter, 2004, 16: 4089−4102.

[19] NEERAJ P, VIKRAM S, PANDVA D K, AGARAWAL S K. Grain boundary effects on the electrical and magnetic properties of $Pr_{2/3}Ba_{1/3}MnO_3$ and $La_{2/3}Ca_{1/3}MnO_3$ manganites [J]. Mater Lett, 2007, 61: 4879−4883.

[20] SAGDEO P R, SHABID Anwar, LALLA N P, PATIL S I. The contribution of grain boundary and defects to the resistivity in the ferromagnetic state of polycrystalline manganites [J]. J Magn Magn Mater, 2006, 306: 60−68.

[21] MITANI S, FUJIMORI H, OHNUMA S. Spin-dependent tunneling phenomena in insulating granular system [J]. J Magn Magn Mater, 1997, 165: 141−148.

[22] MATSOURA M. Nonohmic properties of zinc oxide ceramics [J]. Jpn J Appl Phys, 1971, 10: 736−746.

**(Edited by YUAN Sai-qian)**